Heterogeneous CaMKII-Dependent Synaptic Compensations in CA1 Pyramidal Neurons From Acute Hippocampal Slices

Pablo Vergara†, Gabriela Pino†, Jorge Vera†, Felipe Arancibia and Magdalena Sanhueza*

Cell Physiology Center, Department of Biology, Faculty of Sciences, University of Chile, Santiago, Chile

Prolonged changes in neural activity trigger homeostatic synaptic plasticity (HSP) allowing neuronal networks to operate within functional ranges. Cell-wide or input-specific adaptations can be induced by pharmacological or genetic manipulations of activity, and by sensory deprivation. Reactive functional changes caused by deafferentation may partially share mechanisms with HSP. Acute hippocampal slices are a suitable model to investigate relatively rapid (hours) modifications occurring after denervation and explore the underlying mechanisms. As during slicing many afferents are cut, we conducted whole-cell recordings of miniature excitatory postsynaptic currents (mEPSCs) in CA1 pyramidal neurons to evaluate changes over the following 12 h. As Schaffer collaterals constitute a major glutamatergic input to these neurons, we also dissected CA3. We observed an average increment in mEPSCs amplitude and a decrease in decay time, suggesting synaptic AMPA receptor upregulation and subunit content modifications. Sorting mEPSC by rise time, a correlate of synapse location along dendrites, revealed amplitude raises at two separate domains. A specific frequency increase was observed in the same domains and was accompanied by a global, unspecific raise. Amplitude and frequency increments were lower at sites initially more active, consistent with local compensatory processes. Transient preincubation with a specific Ca^{2+}/calmodulin-dependent kinase II (CaMKII) inhibitor either blocked or occluded amplitude and frequency upregulation in different synapse populations. Results are consistent with the concurrent development of different known CaMKII-dependent HSP processes. Our observations support that deafferentation causes rapid and diverse compensations resembling classical slow forms of adaptation to inactivity. These results may contribute to understand fast-developing homeostatic or pathological events after brain injury.

Keywords: rat brain slices, CA1 pyramidal neurons, deafferentation, homeostatic synaptic plasticity, CaMKII

INTRODUCTION

Homeostatic synaptic plasticity (HSP) consists of compensatory mechanisms adjusting synaptic strength up or down depending on activity levels and maintaining average transmission within a range allowing circuit stability (Turrigiano and Nelson, 2000). Inactivity-induced upregulation of glutamatergic synapses is expressed after long-lasting (typically, 1–2 days) pharmacological

inhibition of action potentials or synaptic transmission (O'Brien et al., 1998; Turrigiano et al., 1998), and in cortical slices from sensory-deprived rodents (Goel et al., 2006; Lee and Kirkwood, 2019).

While pioneer works described a drug-induced cell-wide synaptic scaling, locally regulated homeostatic processes have now been extensively reported (Turrigiano, 2012). Diverse expression mechanisms have been described for adaptation to inactivity. In many cases, they include the specific synaptic incorporation of GluA2-lacking, Ca^{2+}-permeable AMPA receptors (Thiagarajan et al., 2005; Sutton et al., 2006). In others, both GluA1 and GluA2 subunits are upregulated (O'Brien et al., 1998; Wierenga, 2005).

Ca^{2+}/calmodulin-dependent kinase II (CaMKII) is a major component of glutamatergic synapses and is crucial for Hebbian plasticity (Lisman et al., 2012; Hell, 2014; Bayer and Schulman, 2019). In the forebrain, CaMKII holoenzyme is usually formed by 12 subunits of the α and β isoforms (Bennett et al., 1983; Lisman et al., 2012). Both Ca^{2+}-dependent and autonomous CaMKIIα activity (generated by T286 autophosphorylation), and its binding to the glutamate NMDA receptor (NMDAR) are critical for long-term potentiation (LTP). Moreover, the CaMKIIα/NMDAR interaction is involved in synaptic strength maintenance (Sanhueza et al., 2011; Incontro et al., 2018). CaMKII also participates in forms of HSP (Lee, 2012; Hell, 2014). α and β subunits have different affinities for Ca^{2+}/CaM and interact with specific cytoskeletal and postsynaptic density proteins, determining holoenzyme localization in an activity-dependent manner (Hell, 2014). Subunit expression is inversely regulated by neural activity: long-lasting inactivity increases CAMKIIß and decreases CaMKIIα. Moreover, CAMKIIß knockdown or inhibition by the CaMKII inhibitor KN-93 prevents the synaptic upregulation caused by activity blockade (Thiagarajan et al., 2002; Groth et al., 2011). On the other hand, CaMKIIα normally limits AMPAR synaptic incorporation and network silencing disrupts this mechanism, leading to homeostatic upregulation (Wang et al., 2011; Djakovic et al., 2012).

In vivo studies have shown that denervation induces compensatory adaptations in peripheral and central synapses days after deafferentation (Li and Prince, 2002; Houweling et al., 2005; Turrigiano, 2012). Moreover, surgical removal of the entorhinal cortex from slice cultures triggers mEPSC amplitude upregulation in *dentate gyrus* (DG) granule cells; changes take ∼2 days and share signaling properties with forms of drug-induced HSP (Vlachos et al., 2012; Pederiy and Westbrook, 2013; Bissen et al., 2021).

While acute hippocampal slices preserve the local tissue structure, many afferent connections are lost, presumably causing strong activity alterations. Whether homeostatic-like compensations after deafferentation can occur during the lifespan of acute slices requires examination. In addition to the global denervation, it is possible to increase the chance to see reactive changes by cutting synaptic inputs from strong afferent pathways. In intact hippocampal slices action potential-induced release is responsible for ∼25% of spontaneous events on CA1 neurons (including miniature events and action potential-evoked currents), is mainly due to intrinsic CA3 activity, and increases by ∼40% the average event amplitude (Banerjee et al., 2013). Thus, it is reasonable to expect that this specific deafferentation could contribute to the induction of synaptic upregulation in CA1 neurons. Another reason to remove CA3 is that preserving it would not allow us to disregard indirect effects caused by compensatory changes in CA3 neurons after slicing. This is an important issue because previous reports have shown that modifications of DG/CA3/CA1 synapses are specific and do not necessarily follow the conventional rule of homeostasis (Echegoyen et al., 2007; Kim and Tsien, 2008).
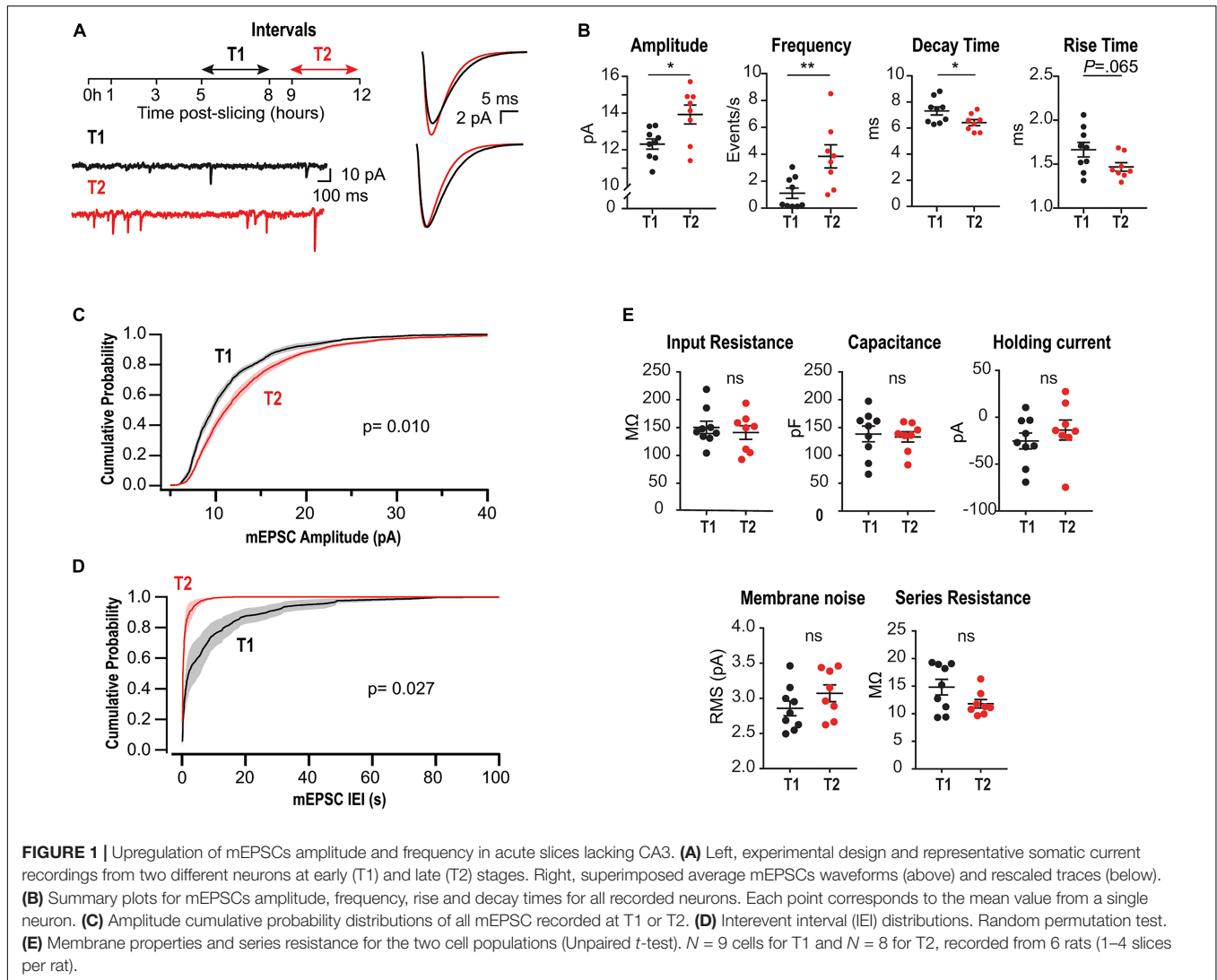
Interestingly, fast (hours) adaptations to inactivity can be triggered by combining the action potential blocker tetrodotoxin (TTX) and NMDAR antagonists (Sutton et al., 2006; Ibata et al., 2008) in cell cultures or acute slices, by a mechanism different from slow forms of HSP. To explore the nature of synaptic changes developed over the lifespan of slices that underwent CA3 dissection, we compared mEPSCs at a relatively early period (5–8 h) with those at a later interval (9–12 h). We observed distance-dependent compensations in mEPSC amplitude and frequency that were differentially affected by CaMKII inhibition. Our evidence supports that the mechanisms underlying these compensations resemble distinct known drug-induced forms of HSP.

MATERIALS AND METHODS

Animal care and experimental procedures were approved by the Bio-Ethics Committee of the Faculty of Sciences, University of Chile, according to the Biosafety Policy Manual of the Fondo Nacional de Desarrollo Científico y Tecnológico (FONDECYT), Chile.

Hippocampal Slice Preparation and Preincubation

Male Sprague–Dawley rats, 18–22 days old, were deeply anesthetized and decapitated. Transverse hippocampal slices (350 μm) were prepared in an ice-cold dissection solution containing (in mM) 125 NaCl, 2.6 KCl, 10 $MgCl_2$, 0.5 $CaCl_2$, 26 $NaHCO_3$, 1.2 NaH_2PO_4, and 10 D-glucose (equilibrated with 95% O_2 and 5% CO_2), pH 7.3. CA3 was surgically removed and slices were transferred to interface chambers (tissue inserts, 8 μm) in an atmosphere saturated with 95% O_2 and 5% CO_2, at 30°C. Each insert held 2–3 slices submerged in a drop of 200 μL artificial cerebrospinal fluid (ACSF) containing (in mM) 125 NaCl, 26 $NaHCO_3$, 1 NaH_2PO_4, 2.6 KCl, 2 $CaCl_2$, 1 $MgCl_2$, and 10 D-glucose. After 1 h, the drop of ACSF was gently replaced by freshly oxygenated solution (for **Figures 1**, **2**). Slices were stored up to 12 h in the interface chambers at 30°C, excepting experiments in **Supplementary Figure 4**, where they were kept at 22°C, after 1 h recovery at 30°C. Recordings were performed 5–12 h after dissection. For peptide preincubations, the solution was replaced by oxygenated ACSF containing CN21 or SCR peptide (5 μM). After 2 h, slices were washed four times and maintained for at least 2 more hours before recordings. As before, recordings were conducted 5–12 h after dissection.

FIGURE 1 | Upregulation of mEPSCs amplitude and frequency in acute slices lacking CA3. **(A)** Left, experimental design and representative somatic current recordings from two different neurons at early (T1) and late (T2) stages. Right, superimposed average mEPSCs waveforms (above) and rescaled traces (below). **(B)** Summary plots for mEPSCs amplitude, frequency, rise and decay times for all recorded neurons. Each point corresponds to the mean value from a single neuron. **(C)** Amplitude cumulative probability distributions of all mEPSC recorded at T1 or T2. **(D)** Interevent interval (IEI) distributions. Random permutation test. **(E)** Membrane properties and series resistance for the two cell populations (Unpaired t-test). $N = 9$ cells for T1 and $N = 8$ for T2, recorded from 6 rats (1–4 slices per rat).

Peptides

The CaMKIIN-derived peptide CN21 fused to the cell-permeable sequence tat (Vest et al., 2007; Sanhueza et al., 2011) and a scrambled control peptide, were obtained from Biomatik (Wilmington, DE, United States).
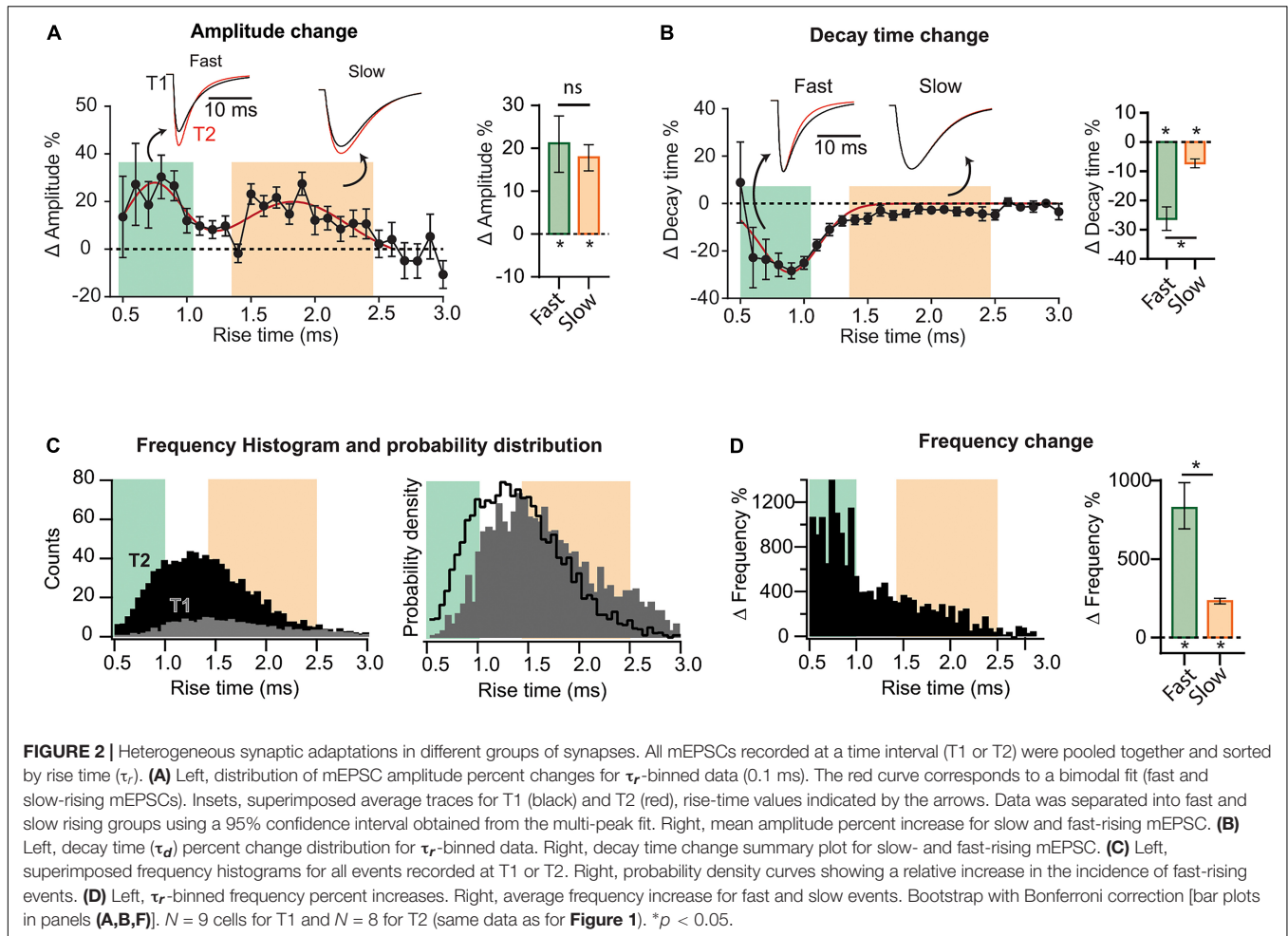
Electrophysiological Recordings

Slices were transferred to a submersion-type recording chamber mounted on an upright microscope (Nikon E600FN) and were continuously superfused (2–4 mL/min) with oxygenated ACSF. A total volume of 100 mL solution was recirculated using a two-way pump. Whole-cell patch-clamp recordings were performed using an EPC-10 amplifier (HEKA Elektronik, Reutlingen, Germany). Patch electrodes (2–5 MΩ) were pulled from borosilicate glass and the internal solution contained (in mM): 115 Cs-methanesulfonate, 20 CsCl, 0.6 EGTA, 10 HEPES, 4 Na_2-ATP, 0.4 Na-GTP, 10 Na_2-phosphocreatine and 2.5 $MgCl_2$ (293 mOsm, pH 7.25). mEPSCs were measured at −60 mV without junction potential (∼12 mV) correction. Recordings

were performed at 30 ± 1°C in the presence of 100 μM picrotoxin (GABA-A inhibitor) and 1 μM TTX. Drugs were only used in the recording chamber to isolate mEPSC. For most of the time, slices were kept in the preincubation chamber in the absence of drugs.

Statistics and Data Processing

Data analysis was done using GraphPad 7 (Prism) and custom-built algorithms designed in IgorPro 8 (Wavemetrics, Inc.). Equality of variance and normality were addressed using the Brown-Forsythe and the Shapiro–Wilk normality test, using an α value of 0.05. In **Figures 2**, **3F,L**, error bars are the 95% confidence interval of the mean. In all other figures error bars are SEM.

Random permutations test: Cumulative probability plots were compared by calculating the maximum absolute distance between the curves obtained after averaging distributions for all neurons recorded at T1 or T2. To evaluate statistical significance, surrogate data were produced by 10,000 random permutations of the cumulative plots.

FIGURE 2 | Heterogeneous synaptic adaptations in different groups of synapses. All mEPSCs recorded at a time interval (T1 or T2) were pooled together and sorted by rise time (τ_r). **(A)** Left, distribution of mEPSC amplitude percent changes for τ_r-binned data (0.1 ms). The red curve corresponds to a bimodal fit (fast and slow-rising mEPSCs). Insets, superimposed average traces for T1 (black) and T2 (red), rise-time values indicated by the arrows. Data was separated into fast and slow rising groups using a 95% confidence interval obtained from the multi-peak fit. Right, mean amplitude percent increase for slow and fast-rising mEPSC. **(B)** Left, decay time (τ_d) percent change distribution for τ_r-binned data. Right, decay time change summary plot for slow- and fast-rising mEPSC. **(C)** Left, superimposed frequency histograms for all events recorded at T1 or T2. Right, probability density curves showing a relative increase in the incidence of fast-rising events. **(D)** τ_r-binned frequency percent increases. Right, average frequency increase for fast and slow events. Bootstrap with Bonferroni correction [bar plots in panels **(A,B,F)**]. $N = 9$ cells for T1 and $N = 8$ for T2 (same data as for **Figure 1**). *$p < 0.05$.

Bootstrap with weighted p-value: To compare rise-time-binned data in **Figure 4**, a *p*-value was calculated for each bin with the percentile bootstrap test. Family-wise error rate was corrected by multiplying each *p*-value by that of adjacent neighbors. This maintains family-wise error below 5% and preserves regional inference (Yang et al., 2001).

RESULTS

To evaluate time-dependent synaptic adaptations in CA1 pyramidal neurons from acute slices lacking CA3, we recorded mEPSCs at two different intervals after preparation: T1 (5–8 h) and T2 (9–12 h) (**Figure 1A**, left). Earlier than 5 h, mEPSCs frequency was too low to perform statistical analyses. **Figure 1A**, right, displays the overlaid average mEPSC waveforms for all events recorded at T1 or T2, and their rescaled version (below) suggesting modifications in amplitude and kinetics. Accordingly, summary plots in **Figure 1B** show a significant increase in amplitude and a decrease in decay time, each point corresponds to the mean value from one cell. Moreover, a strong increase in average frequency was demonstrated. **Figures 1C,D** display amplitude and frequency cumulative probability distributions,

respectively, for T1 and T2 (see summary data and statistics for **Figure 1** in **Supplementary Table 1**). These results are consistent with a compensatory process tending to gradually recover transmission in CA1 neurons after the abrupt decrease in activity by slicing and CA3 dissection. Interestingly, in classical studies of HSP a decrease in decay time has been associated with the insertion of GluA2-lacking receptors displaying faster decay kinetics (Geiger et al., 1995; Turrigiano, 2008; Lee, 2012).

To optimize slices health during such long incubation times, we used interface chambers (Gibb and Edwards, 1994; Lipton et al., 1995). We checked for possible alterations in neuronal membrane properties after long-lasting storage, finding that passive properties, holding current, and membrane noise were similar for T1 and T2 (**Figure 1E**). Moreover, there was no significant change in series resistance or correlation with mEPSC kinetics (**Supplementary Figure 1**). Thus, changes in mEPSCs cannot be attributed to time-dependent modifications in these variables.

Recent studies have identified different subpopulations of CA1 neurons with distinct biophysical and morphological properties. Hypothetically, some subpopulations could preferentially survive until T2, which would generate a bias in the average variables. To evaluate this possibility, we projected all the recorded
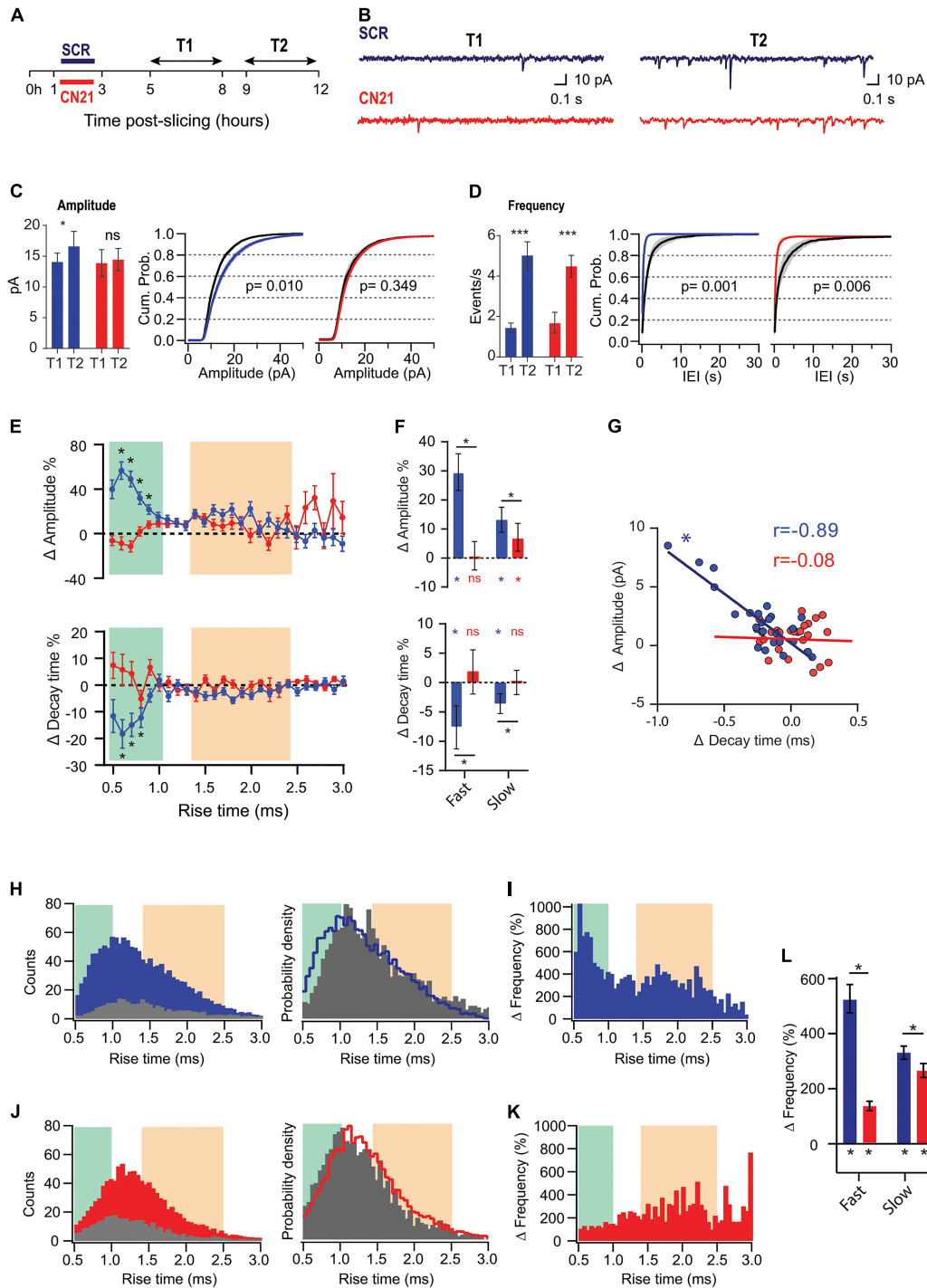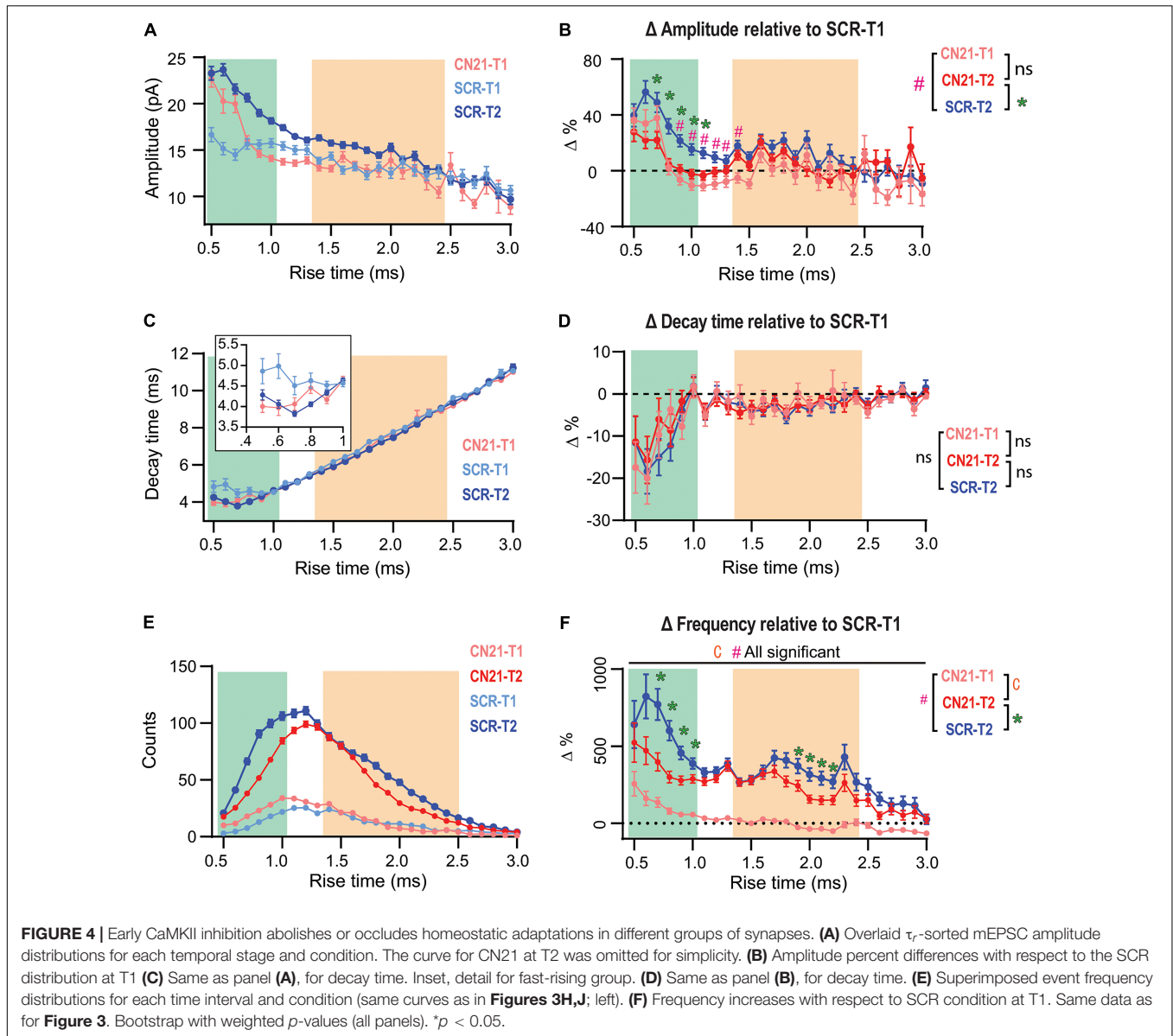
FIGURE 3 | CaMKII is involved in different adaptations in acute slices. **(A)** Experimental design. Slices were preincubated for 2 h with CN21 or SCR peptide and drugs were washed out for 2 h (T1 and T2 are the same as for **Figures 1**, **2**). **(B)** Representative current traces recorded at T1 and T2 in each condition **(C)** Mean mEPSCs amplitudes at T1 and T2 (left) and overlaid cumulative probability curves for CN21 (center) and SCR (right), including all mEPSCs recorded during each period. Black curves: distributions at T1. Two-way ANOVA with Bonferroni correction for bar plot, random permutations for cumulative probability plots. **(D)** Same as panel **(C)** for mEPSCs frequency and interevent interval (IEI). **(E)** Percent changes in amplitude and decay time for τ_r-binned data. Bootstrap with weighted P-values. **(F)** Average amplitude and decay time percent changes for slow and fast-rising groups. Bootstrap with Bonferroni correction. **(G)** Amplitude vs. decay time raw changes for CN21 or SCR peptide. Each point corresponds to the average change for τ_r bin. Pearson correlation. **(H)** Frequency histograms (left) for all events recorded at T1 or T2 and probability density curve (right), in SCR condition. **(I)** τ_r-binned frequency percent increase. **(J,K)** Same as **(H,I)**, for CN21. **(L)** Average frequency increase for fast and slow groups, after SCR or CN21. Bootstrap with Bonferroni correction. *$p < 0.05$. $N = 39$ neurons (SCR-T1: 11, SCR-T2: 8, CN21-T1: 8, CN21-T2: 12), from 5 rats (1–4 slices per rat).

FIGURE 4 | Early CaMKII inhibition abolishes or occludes homeostatic adaptations in different groups of synapses. **(A)** Overlaid τ_r-sorted mEPSC amplitude distributions for each temporal stage and condition. The curve for CN21 at T2 was omitted for simplicity. **(B)** Amplitude percent differences with respect to the SCR distribution at T1 **(C)** Same as panel **(A)**, for decay time. Inset, detail for fast-rising group. **(D)** Same as panel **(B)**, for decay time. **(E)** Superimposed event frequency distributions for each time interval and condition (same curves as in **Figures 3H,J**; left). **(F)** Frequency increases with respect to SCR condition at T1. Same data as for **Figure 3**. Bootstrap with weighted p-values (all panels). *$p < 0.05$.

electrophysiological properties into a two-dimensional plane displaying the maximum separation between T1 and T2 (partial least squares-discriminant analysis, PLS-DA). Most of the neurons recorded in T2 were outside the 95% boundary of the neurons recorded in T1 (**Supplementary Figure 2**). This indicates that the neurons recorded at T2 had properties that could not be found in T1 and therefore emerged as a time-dependent process.

The changes in average amplitude and frequency for all neurons recorded along slices lifespan are depicted in **Supplementary Figure 3**. Although it is possible to record before 5 h, several neurons would display zero frequency or too few events to reliably estimate average mEPSC amplitude and kinetics. Therefore, to avoid a biased sampling at T1, recordings were done after 5 h. Interestingly, we observed that synaptic upregulation was strongly dependent on the temperature at

which slices were stored. As shown in **Supplementary Figure 4**, average amplitude increase was abolished after incubation at room temperature (22°C) and frequency increase was strongly reduced.

To explore possible differential adaptations along the dendritic tree, we sorted all recorded mEPSCs by their rise time (τ_r), which is positively correlated to the distance to the soma (Letzkus et al., 2006; Sjöström and Häusser, 2006). mEPSCs were grouped and averaged in τ_r bins (0.1 ms) to then compute the changes between T1 and T2. This analysis revealed that percent increase in amplitude followed a bimodal distribution (**Figure 2A**), possibly involving two separated synapse groups. A third population ($\tau_r > \sim 2.5$ ms), presumably located more distally, did not display detectable changes. To quantify the average change in amplitude for each population, we established a quantitative criterium to classify as "fast" or "slow" the

points in the distribution. Data was separated into two groups delimited by a 95% confidence interval, obtaining the following limits: fast population, $\tau_r \leq 1$ ms (green) and slow population, 1.4 ms $\leq \tau_r \leq 2.5$ ms (pink). See **Supplementary Figure 5** for details on this procedure. Events lying in the transition among the two groups (1.0 ms $\leq \tau_r \leq 1.4$ ms) cannot be classified as belonging to a specific group. Note that the definition of slow or fast-rising events follows from the way the amplitude changes and not from the amplitude distribution itself at a specific time. The insets in **Figure 2A** show superimposed average mEPSCs at T1 and T2, calculated from all events in each population. mEPSCs amplitude increase was significant for both fast and slow groups (**Figure 2A**, right), with no statistical difference between them (see summary data and statistics for **Figure 2** in **Supplementary Table 2**). Comparing the decay time (τ_d) as a function of τ_r, evident changes for the fast-rising group were revealed, while the second population presented a very small (but significant) modification (**Figure 2B**).

To examine whether the increase in frequency followed a particular pattern, we constructed histograms of event counts as a function of τ_r, at T1 and T2. Superimposed curves (**Figure 2C**, left) demonstrated a strong and widespread increment in mEPSC occurrence. Both distributions display a single peak, however, the probability density distributions (**Figure 2C**, right), revealed a shift to the left at T2. Therefore, while the occurrence of both fast and slow-rising mEPSCs strongly increased with time, it was more probable to observe faster than slower events at T2 compared to T1. In line with this result, percent frequency increase was substantially higher in the lower τ_r range (**Figure 2D**). With regards to the slowest events ($\tau_r > 2.5$ ms), the increase was negligible. Interestingly, amplitude increases were lower in the domain displaying the highest frequencies at T1, consistent with a homeostatic-like effect.

Because amplitudes and frequencies vary differentially, the change in the contribution of each population are not straightforward to appreciate. **Supplementary Figures 6A,C** shows amplitude and frequency distributions per rise time at T1 and T2 (from which the changes of **Figure 2** were calculated). The average amplitude and frequency values of fast, slow, and intermediate (unclassified) events are also shown for T1 and T2 (**Supplementary Figures 6B,D**). Finally, as an attempt to quantify and compare synapses reorganization in the different domains, we calculated a weighted average considering both event amplitude and frequency (**Supplementary Figure 6E**). Overall, these results indicate that while both amplitude and frequency increased in the three groups, the total weight of the fast population, presumably located more proximally, grew at the expense of the other two groups.

To address whether CaMKII mediates synaptic adaptations in our slices as it does in some known forms of HSP, we inhibited the holoenzyme using the CN21 peptide, a 21 amino-acid sequence derived from an endogenous protein, a specific and efficient CaMKII inhibitor. After recovery, the slices were incubated for 2 h with cell-permeable, tat-fused CN21 (**Figure 3A**) to inhibit CaMKII activity during the early post-denervation period. A second group of slices was treated with a scrambled control peptide (SCR). After washing out the drugs for at least 2 h, we conducted interleaved mEPSCs recordings for each condition at the same T1 and T2 intervals, as for previous experiments. As shown in **Figure 3C** (left), the increase in mEPSC amplitude also developed after SCR but was abolished by CN21, as calculated by averaging the mean values from each cell (see summary data and statistics for **Figure 3** in **Supplementary Table 3**). Moreover, after active peptide incubation the cumulative probability curves at T1 and T2 were not statistically different (**Figure 3C**, right). In contrast, an increase in average frequency was detected in both conditions (**Figure 3D**).

Analysis of τ_r-sorted mEPSCs amplitude changes revealed that incubation with CN21 abolished upscaling of fast-rising mEPSCs and significantly reduced it for the slow-rising group (**Figures 3E,F**; upper panels). In addition, CN21 prevented τ_d decrease for both populations (lower panels). These observations support a role of CaMKII in mEPSCs upscaling and suggest that this regulation may involve the incorporation of GluA2-lacking receptors. Consistent with this possibility, we found a linear inverse correlation between amplitude increases and τ_d decreases (**Figure 3G**), suggesting a shared signaling pathway. This correlation was missing after CN21 incubation.

Examination of τ_r-sorted mEPSCs frequencies revealed that while an upregulation was observed after both SCR and CN21, the distribution was quite different (**Figures 3H–K**). The strong increase in frequency of fast-rising events was decreased by CN21, falling below the level of the slow group (**Figures 3I,K,L**). In addition, the incidence of slow events was also dampened after CN21. These results point to the existence of both CaMKII-dependent and independent mechanisms underlying the frequency raise.

In summary, we detected CaMKII-related synaptic compensations developing hours after dissection. Interestingly, a closer examination of these reactive adjustments revealed further complexities consistent with the existence of different CaMKII-related mechanisms. We will next show that early kinase inhibition produced either suppression or occlusion of changes in separate synapse populations.

So far, we had focused on quantifying changes between two time periods (T1 and T2) in slices treated with either active or control peptides. However, Dumas et al. (2018) reported that dissection of CA3 caused fEPSP upregulation after ~3 h, thus, some synaptic changes could be already in course at T1 in our slices. Therefore, we compared the amplitude distributions for SCR- and CN21-incubated slices at T1 (**Figure 4A**, light blue and pink traces) and included the control curve at T2 for comparison (blue trace). At T1 the curves clearly differ for some τ_r domains (see details on statistics in **Supplementary Figure 7A**). Intriguingly, a subgroup of the mEPSCs displaying the fastest rising kinetics were already augmented at T1 after CN21. On the other hand, a different population was lower than control. To visualize and quantify changes among conditions and time, we plotted the amplitude differences relative to the control at T1, now also including the curve for CN21 at T2 (**Figure 4B**). The results suggest that CaMKII inhibition promoted the earlier development of amplitude compensations in part of the fast-rising population and in the slow group. Consistent with **Figure 3E**, early and late curves from CN21-treated slices did

not differ, but this may be due to two different phenomena: first, an occlusion effect over the fastest subpopulation and the slow group; second, a proper inhibition of the amplitude increase for an intermediate group. A similar analysis of decay times (**Figures 4C,D**) also suggests a faster reorganization in AMPARs subunit composition after CN21.

Regarding frequency changes, **Figure 4E** displays overlaid histograms (same as in **Figures 3H,J**; left) and **Figure 4F** the percent differences relative to control at T1. Again, after CN21 the increase in frequency of the faster synaptic events appeared to start earlier (pink traces in **Figure 4F** and **Supplementary Figure 7C**). However, the difference between pink and red curves in **Figure 4F** confirms that frequency upregulation also included a global CaMKII-independent mechanism. Finally, comparing these curves with the control increment (**Figure 4F**, blue curve) reveals that CN21 also inhibits a frequency increase depending on CaMKII and involving both fast and slow-rising events. Interestingly, like the amplitude increases, CaMKII-sensitive frequency changes were higher for synapses with lower incidence at T1 and were practically absent in the more abundant population, suggesting that the compensatory changes observed in our model of tissue denervation resemble homeostatic plasticity mechanisms involving CaMKII.

DISCUSSION

We examined mEPSCs changes along the lifespan of acute slices that underwent CA3 removal during the slicing procedure. These compensations did not require pharmacological manipulations, were differentially expressed along dendrites, and involved distinct CaMKII-related regulations. Our results support that acute denervation can rapidly induce, in a single neuron, different synaptic adjustments resembling classical forms of adaptation to inactivity.

Average mEPSCs amplitude and frequency increased over early (T1, 5–8 h) and late (T2, 9–12 h) stages. As earlier than 5 h synaptic activity was very low, these changes are consistent with an ongoing inactivity-induced compensatory process. To investigate the underlying mechanisms, we sorted mEPSCs by their rise time (τ_r), which depends on dendritic filtering and provides an estimate of the relative distance to the soma. mEPSCs presumably originating at separate regions of the dendritic tree followed non-uniform rules and the domains with higher activity levels at T1 developed lower amplitude and frequency increases, consistent with locally regulated compensatory phenomena.

The mean amplitude increase was accompanied by a decrease in decay time (τ_d), which is usually interpreted as a rise in the proportion of GluA2-lacking receptors, due to their faster deactivation/desensitization kinetics (Geiger et al., 1995). Moreover, amplitude and decay time changes displayed a linear inverse correlation, further suggesting a major contribution of this type of AMPARs to synaptic strength upregulation. Interestingly, several lines of evidence support a role for GluA2-lacking AMPARs in homeostatic upregulations after long-lasting neuronal activity silencing, including pharmacological manipulations, sensory deprivation, and inhibition of glutamate

release at single synapses (Ju et al., 2004; Thiagarajan et al., 2005; Goel et al., 2006; Hou et al., 2008; Beique et al., 2011; Groth et al., 2011). A similar mechanism underlies the faster compensations triggered by simultaneous action potential and NMDAR inhibition (Sutton et al., 2006; Wang et al., 2011).

Overall, our observations are consistent with the development of synaptic upregulation mechanisms in distinct populations of synapses along CA1 neuron dendrites along the lifespan of the slices. As Schaffer collaterals provide a major input to these cells and CA3 removal was shown to increase evoked field potentials in acute slices ∼3 h after dissection (Dumas et al., 2018), the changes we observed could be in part due to this pathway-specific deafferentation. Moreover, an increase in GluA1 content was detected by immunohistochemistry in *stratum radiatum* after CA3 dissection, compared to slices preserving this region (Dumas et al., 2018). Interestingly, we did not detect amplitude changes for the slowest-rising population (τ_r higher than ∼2.5 ms). This result was not due to insufficient technical resolution to detect changes at distant synapses, as the amplitudes of these events (∼12 pA) were more than twice our detection threshold and only slightly lower than populations displaying significant upregulation. It is possible to speculate that this population could mainly correspond to the most distal region of CA1 apical dendrites at the *stratum lacunosum moleculare*, that do not receive inputs from CA3. Determining to what extent the changes observed here are dependent on CA3 deletion or on isolation of the tissue from the rest of the brain requires further investigation.

We observed a global rise in mEPSC frequency, but increases were higher at the loci where amplitude changes occurred, consistent with both specific and unspecific frequency compensations. Some studies of adaptations to inactivity have reported frequency increases (Thiagarajan et al., 2005; Echegoyen et al., 2007; Groth et al., 2011) and may involve an enlargement of presynaptic terminals or an increase in vesicle pools and turnover (Bacci et al., 2001; Murthy et al., 2001). Interestingly, release probability can be homeostatically regulated by the local dendritic activity (Branco et al., 2008), consistent with a lower frequency increase at originally more active synapses. Also, dendrites extend new spine head protrusions after 2 h of network silencing in slice cultures (Richards et al., 2005). An overall increase in spine density and multiple-synapse boutons occur in CA1 neurons hours after slice preparation (Kirov et al., 1999). Moreover, drug-induced silencing triggered widespread spine increases in slices (Kirov and Harris, 1999). Because in these studies CA3 was preserved, the cell-wide frequency increase observed here may be partly due to a general synapse upregulation triggered by the slicing procedure itself.

Different lines of evidence relate CaMKII with slow drug-induced adaptation to inactivity. Low Ca^{2+} levels preferentially activate CaMKIIβ, and knockdown of this subunit or general CaMKII pharmacological inhibition abolished mEPSC amplitude and frequency rise, supporting a specific role of ß in this form of HSP (Thiagarajan et al., 2002; Groth et al., 2011). Consistently, CaMKIIβ-dependent phosphorylation of the AMPAR regulatory protein stargazin

is required for receptor incorporation to synapses (Louros et al., 2014). Moreover, phosphorylation of the guanylate-kinase-associated protein (GKAP) by CaMKIIβ boosts its synaptic accumulation and assembling of a scaffold complex with PSD-95 and Shank (Naisbitt et al., 1999; Shin et al., 2012; Rasmussen et al., 2017). However, the decrease in CaMKIIα activity during network silencing may also contribute to homeostatic upregulation. Normally, GKAP phosphorylation by CaMKIIα promotes its removal from synapses, limiting synaptic strength. Moreover, CaMKIIα-dependent proteosome recruitment causes degradation of GKAP and other scaffolds, destabilizing receptors and mimicking activity-induced downscaling (Bingol et al., 2010; Djakovic et al., 2012; Rasmussen et al., 2017). Therefore, while CaMKIIβ may trigger synaptic upregulation, CaMKIIα activity is expected to restrict transmission levels.

In consequence, it seems reasonable to propose that we are observing two different types of CaMKII-dependent fast homeostatic synaptic compensations. Early CN21 application blocked the changes requiring CaMKII activity, consistent with the known CaMKIIβ-mediated mechanism. On the other hand, CaMKII inhibition hastened other compensatory changes, in line with an alteration of the CaMKIIα-dependent mechanism limiting synaptic strength. If this interpretation is correct, the question arises on the factors determining which mechanism is expressed or prevails in different synapses.

It could be hypothesized that the effects observed here recapitulate, in part, the fast-developing HSP induced by TTX + APV (Sutton et al., 2006; Wang et al., 2011). These fast adaptations critically depend on CaMKIIα autophosphorylation and its binding to NMDAR in cortical neurons (Wang et al., 2011), thus CN21 application could be mimicking NMDAR blockade. Moreover, action potential-induced glutamate release on CA1 pyramidal neurons is mainly due to CA3 neurons activity (Banerjee et al., 2013). Interestingly, mEPSC upregulation by TTX + APV involves locally translated GluA2-lacking receptors, allowing rapid and specific adjustments (Ju et al., 2004; Sutton et al., 2006). Even individual synapses can autonomously compensate for neurotransmitter decreases (Ju et al., 2004; Hou et al., 2008; Beique et al., 2011), and Ca^{2+} entry through GluA2-lacking AMPARs can retrogradely increase vesicle turnover (Lindskog et al., 2010). The decay time shortening and differential changes along dendrites in our slices are consistent with these homeostatic mechanisms, and it could be hypothesized that a similar coordination among pre and postsynaptic modifications may underlie the coincident increase in amplitude and frequency observed here in groups of synapses. However, we also detected CN21-sensitive changes lacking a decay time reduction that may not rely on GluA2-lacking receptors. Further research is needed to assess these questions.

It should be noted that in conjunction with the homeostatic compensation in the excitatory inputs, adaptations of inhibitory neurotransmission could also take place (Karmarkar and Buonomano, 2006). Long-lasting reduction in interneurons activity and the following time-dependent compensations could have complex effects at network level and influence excitatory inputs to CA1 neurons. While we cannot discard this possibility, a work comparing mIPSCs amplitude and frequency in acute slices shortly after dissection reported no significant differences among slices containing or devoid of CA3 (Banerjee et al., 2013), in contrast to mEPSC. Still, possible compensations related to tissue isolation from the rest of the brain could occur. While mEPSC rise-time depends on synapse distance to the soma, other factors as dendrite diameter and branching may also affect this variable, and it is not straightforward to predict the relative position of synapses. While apical spine density in CA1 neurons is highest at the distal third of *stratum radiatum,* synapses are also abundant at basal dendrites, innervated by Schaffer collaterals as well (Megìas et al., 2001). These questions should be addressed in future studies.

Interestingly, CN21 peptide derives from the CaMKIIN protein, a specific endogenous inhibitor of CaMKII (Chang et al., 1998; Vest et al., 2007), whose function is not well understood, but has been associated with Hebbian synaptic plasticity and memory (Sanhueza et al., 2011; Gouet et al., 2012; Vigil et al., 2017). Notably, the CaMKIIN gene is rapidly regulated after LTP induction (Astudillo et al., 2020). Therefore, our results may contribute to understand possible CaMKIIN-dependent regulatory processes.

To the best of our knowledge, denervation-induced fast synaptic changes following similar rules than known forms of HSP had not been demonstrated. Moreover, the simultaneous occurrence in neurons of different homeostatic processes has not been reported. HSP studies usually compare control and test conditions at a similar time stage, in contrast to our work that investigates the development of changes over time. The study of ongoing adaptations occurring in slices may contribute to unraveling rapid pathway-specific mechanisms and understanding reactive phenomena following brain injury.

Finally, researchers should be aware that synaptic compensations can occur over the lifespan of slices, possibly affecting results interpretation.

DATA AVAILABILITY STATEMENT

The raw data supporting the conclusions of this article will be made available by the authors, without undue reservation.

ETHICS STATEMENT

The animal study was reviewed and approved by Bio-Ethics Committee of the Faculty of Sciences, University of Chile, according to the Biosafety Policy Manual of the Fondo Nacional de Desarrollo Científico y Tecnológico (FONDECYT), Chile.

AUTHOR CONTRIBUTIONS

PV performed most of the experiments, made the analysis, actively participated in experimental design and results interpretation, and wrote the first draft of the manuscript. GP, JV,

and FA contributed to the experiments and results discussion. MS conducted research conceptualization and design and wrote the final version of the manuscript. All authors contributed to the article and approved the submitted version.

SUPPLEMENTARY MATERIAL

The Supplementary Material for this article can be found online at: https://www.frontiersin.org/articles/10.3389/fncel.2022.821088/full#supplementary-material

REFERENCES

Astudillo, D., Karmelic, D., Casas, B. S., Otmakhov, N., Palma, V., and Sanhueza, M. (2020). CaMKII inhibitor 1 (CaMK2N1) mRNA is upregulated following LTP induction in hippocampal slices. *Synapse* 74:e22158. doi: 10.1002/syn.22158

Bacci, A., Coco, S., Pravettoni, E., Schenk, U., Armano, S., Frassoni, C., et al. (2001). Chronic blockade of glutamate receptors enhances presynaptic release and downregulates the interaction between synaptophysin-synaptobrevin–vesicle-associated membrane protein 2. *J. Neurosci.* 21, 6588–6596. doi: 10.1523/JNEUROSCI.21-17-06588.2001

Banerjee, J., Alkondon, M., Albuquerque, E. X., and Pereira, E. F. R. (2013). Contribution of CA3 and CA1 pyramidal neurons to the tonic α7 nAChR-dependent glutamatergic input to CA1 pyramidal neurons. *Neurosci. Lett.* 554, 167–171. doi: 10.1016/j.neulet.2013.08.025

Bayer, K. U., and Schulman, H. (2019). CaM Kinase: still inspiring at 40. *Neuron* 103, 380–394. doi: 10.1016/j.neuron.2019.05.033

Beique, J.-C., Na, Y., Kuhl, D., Worley, P. F., and Huganir, R. L. (2011). Arc-dependent synapse-specific homeostatic plasticity. *Proc. Natl. Acad. Sci. U.S.A.* 108, 816–821. doi: 10.1073/pnas.1017914108

Bennett, M., Erondu, N., and Kennedy, M. (1983). Purification and characterization of a calmodulin-dependent protein kinase that is highly concentrated in brain. *J. Biol. Chem.* 2, 12735–12744. doi: 10.1016/s0021-9258(17)44239-6

Bingol, B., Wang, C.-F., Arnott, D., Cheng, D., Peng, J., and Sheng, M. (2010). Autophosphorylated CaMKIIα acts as a scaffold to recruit proteasomes to dendritic spines. *Cell* 140, 567–578. doi: 10.1016/j.cell.2010.01.024

Bissen, D., Kracht, M. K., Foss, F., Hofmann, J., and Acker-Palmer, A. (2021). EphrinB2 and GRIP1 stabilize mushroom spines during denervation-induced homeostatic plasticity. *Cell. Rep.* 34:108923. doi: 10.1016/j.celrep.2021.108923

Branco, T., Staras, K., Darcy, K. J., and Goda, Y. (2008). Local dendritic activity sets release probability at hippocampal synapses. *Neuron* 59, 475–485. doi: 10.1016/J.NEURON.2008.07.006

Chang, B. H., Mukherji, S., and Soderling, T. R. (1998). Characterization of a calmodulin kinase II inhibitor protein in brain. *Proc. Natl. Acad. Sci. U. S. A.* 95, 10890–10895. doi: 10.1073/pnas.95.18.10890

Djakovic, S. N., Marquez-Lona, E. M., Jakawich, S. K., Wright, R., Chu, C., Sutton, M. A., et al. (2012). Phosphorylation of Rpt6 Regulates Synaptic Strength in Hippocampal Neurons. *J. Neurosci.* 32, 5126–5131. doi: 10.1523/JNEUROSCI.4427-11.2012

Dumas, T. C., Uttaro, M. R., Barriga, C., Brinkley, T., Halavi, M., Wright, S. N., et al. (2018). Removal of area CA3 from hippocampal slices induces postsynaptic plasticity at Schaffer collateral synapses that normalizes CA1 pyramidal cell discharge. *Neurosci. Lett.* 678, 55–61. doi: 10.1016/j.neulet.2018.05.011

Echegoyen, J., Neu, A., Graber, K. D., and Soltesz, I. (2007). Homeostatic plasticity studies using in vivo hippocampal activity-blockade: synaptic scaling, intrinsic plasticity and age-dependence. *PLoS One* 2:e700. doi: 10.1371/journal.pone.0000700

Geiger, J. R. P., Melcher, T., Koh, D.-S., Sakmann, B., Seeburg, P. H., Jonas, P., et al. (1995). Relative abundance of subunit mRNAs determines gating and Ca^{2+} permeability of AMPA receptors in principal neurons and interneurons in rat CNS. *Neuron* 15, 193–204. doi: 10.1016/0896-6273(95)90076-4

Gibb, A. J., and Edwards, F. A. (1994). Patch clamp recording from cells in sliced tissues. *Microelectrode Tech.* 255–274.

Goel, A., Jiang, B., Xu, L. W., Song, L., Kirkwood, A., and Lee, H.-K. (2006). Cross-modal regulation of synaptic AMPA receptors in primary sensory cortices by visual experience. *Nat. Neurosci.* 9, 1001–1003. doi: 10.1038/nn1725

Gouet, C., Aburto, B., Vergara, C., and Sanhueza, M. (2012). On the mechanism of synaptic depression induced by CaMKIIN, an endogenous inhibitor of CaMKII. *PLoS One* 7:1080630. doi: 10.1371/journal.pone.0049293

Groth, R. D., Lindskog, M., Thiagarajan, T. C., Li, L., and Tsien, R. W. (2011). β $Ca2+$/CaM-dependent kinase type II triggers upregulation of GluA1 to coordinate adaptation to synaptic inactivity in hippocampal neurons. *Proc. Natl. Acad. Sci. U.S.A.* 108, 828–833. doi: 10.1073/pnas.1018022108

Hell, J. W. (2014). CaMKII: claiming center stage in postsynaptic function and organization. *Neuron* 81, 249–265. doi: 10.1016/j.neuron.2013.12.024

Hou, Q., Zhang, D., Jarzylo, L., Huganir, R. L., and Man, H.-Y. (2008). Homeostatic regulation of AMPA receptor expression at single hippocampal synapses. *Proc. Natl. Acad. Sci. U.S.A.* 105, 775–780. doi: 10.1073/pnas.0706447105

Houweling, A. R., Bazhenov, M., Timofeev, I., Steriade, M., and Sejnowski, T. J. (2005). Homeostatic synaptic plasticity can explain post-traumatic epileptogenesis in chronically isolated neocortex. *Cereb. Cortex* 15, 834–845. doi: 10.1093/cercor/bhh184

Ibata, K., Sun, Q., and Turrigiano, G. G. (2008). Rapid synaptic scaling induced by changes in postsynaptic firing. *Neuron* 57, 819–826. doi: 10.1016/j.neuron.2008.02.031

Incontro, S., Díaz-Alonso, J., Iafrati, J., Vieira, M., Asensio, C. S., Sohal, V. S., et al. (2018). The CaMKII/NMDA receptor complex controls hippocampal synaptic transmission by kinase-dependent and independent mechanisms. *Nat. Commun.* 9:2069. doi: 10.1038/s41467-018-04439-7

Ju, W., Morishita, W., Tsui, J., Gaietta, G., Deerinck, T. J., Adams, S. R., et al. (2004). Activity-dependent regulation of dendritic synthesis and trafficking of AMPA receptors. *Nat. Neurosci.* 7, 244–253. doi: 10.1038/nn1189

Karmarkar, U. R., and Buonomano, D. V. (2006). Different forms of homeostatic plasticity are engaged with distinct temporal profiles. *Eur. J. Neurosci.* 23, 1575–1584. doi: 10.1111/j.1460-9568.2006.04692.x

Kim, J., and Tsien, R. W. (2008). Synapse-Specific adaptations to inactivity in hippocampal circuits achieve homeostatic gain control while dampening network reverberation. *Neuron* 58, 925–937. doi: 10.1016/j.neuron.2008.05.009

Kirov, S. A., and Harris, K. M. (1999). Dendrites are more spiny on mature hippocampal neurons when synapses are inactivated. *Nat. Neurosci.* 2, 878–883. doi: 10.1038/13178

Kirov, S. A., Sorra, K. E., and Harris, K. M. (1999). Slices have more synapses than perfusion-fixed hippocampus from both young and mature rats. *J. Neurosci.* 19, 2876–2886. doi: 10.1523/JNEUROSCI.19-08-02876.1999

Lee, H.-K. (2012). Ca2+-permeable AMPA receptors in homeostatic synaptic plasticity. *Front. Mol. Neurosci.* 5:17. doi: 10.3389/fnmol.2012.00017

Lee, H.-K., and Kirkwood, A. (2019). Mechanisms of homeostatic synaptic plasticity in vivo. *Front. Cell. Neurosci* 13:530. doi: 10.3389/fncel.2019.00520

Letzkus, J. J., Kampa, B. M., and Stuart, G. J. (2006). Learning rules for spike timing-dependent plasticity depend on dendritic synapse location. *J. Neurosci.* 26, 10420–10429. doi: 10.1523/JNEUROSCI.2650-06.2006

Li, H., and Prince, D. A. (2002). Synaptic activity in chronically injured. Epileptogenic sensory-motor neocortex. *J. Neurophysiol.* 88, 2–12. doi: 10.1152/jn.00507.2001

Lindskog, M., Li, L., Groth, R. D., Poburko, D., Thiagarajan, T. C., Han, X., et al. (2010). Postsynaptic GluA1 enables acute retrograde enhancement of

presynaptic function to coordinate adaptation to synaptic inactivity. *Proc. Natl. Acad. Sci. U.S.A.* 107, 21806–21811. doi: 10.1073/pnas.1016399107

Lipton, P., Aitken, P. G., Dudek, F. E., Eskessen, K., Espanol, M. T., Ferchmin, P. A., et al. (1995). Making the best of brain slices; comparing preparative methods. *J. Neurosci. Methods* 59, 151–156. doi: 10.1016/0165-0270(94)00205-U

Lisman, J., Yasuda, R., and Raghavachari, S. (2012). Mechanisms of CaMKII action in long-term potentiation. *Nat. Rev. Neurosci.* 13, 169–182. doi: 10.1038/nrn3192

Louros, S. R., Hooks, B. M., Litvina, L., Carvalho, A. L., and Chen, C. (2014). A role for stargazin in experience-dependent plasticity. *Cell Rep.* 7, 1614–1625. doi: 10.1016/J.CELREP.2014.04.054

Megìas, M., Emri, Z., Freund, T., and Gulyás, A. (2001). Total number and distribution of inhibitory and excitatory synapses on hippocampal CA1 pyramidal cells. *Neuroscience* 102, 527–540. doi: 10.1016/S0306-4522(00)00496-6

Murthy, V. N., Schikorski, T., Stevens, C. F., and Zhu, Y. (2001). Inactivity produces increases in neurotransmitter release and synapse size. *Neuron* 32, 673–682. doi: 10.1016/S0896-6273(01)00500-1

Naisbitt, S., Kim, E., Tu, J. C., Xiao, B., Sala, C., Valtschanoff, J., et al. (1999). Shank, a novel family of postsynaptic density proteins that binds to the NMDA receptor/PSD-95/GKAP complex and cortactin. *Neuron* 23, 569–582. doi: 10.1016/S0896-6273(00)80809-0

O'Brien, R. J., Kamboj, S., Ehlers, M. D., Rosen, K. R., Fischbach, G. D., and Huganir, R. L. (1998). Activity-dependent modulation of synaptic AMPA receptor accumulation. *Neuron* 21, 1067–1078. doi: 10.1016/S0896-6273(00)80624-8

Perederiy, J. V., and Westbrook, G. L. (2013). Structural plasticity in the dentate gyrus- revisiting a classic injury model. *Front. Neural Circuits* 7:17. doi: 10.3389/fncir.2013.00017

Rasmussen, A. H., Rasmussen, H. B., and Silahtaroglu, A. (2017). The DLGAP family: neuronal expression, function and role in brain disorders. *Mol. Brain* 10:43. doi: 10.1186/s13041-017-0324-9

Richards, D. A., Mateos, J. M., Hugel, S., de Paola, V., Caroni, P., Gähwiler, B. H., et al. (2005). Glutamate induces the rapid formation of spine head protrusions in hippocampal slice cultures. *Proc. Natl. Acad. Sci. U. S. A.* 102, 6166–61671. doi: 10.1073/pnas.0501881102

Sanhueza, M., Fernandez-Villalobos, G., Stein, I. S., Kasumova, G., Zhang, P., Bayer, K. U., et al. (2011). Role of the CaMKII/NMDA receptor complex in the maintenance of synaptic strength. *J. Neurosci.* 31, 9170–9178. doi: 10.1523/JNEUROSCI.1250-11.2011

Shin, S. M., Zhang, N., Hansen, J., Gerges, N. Z., Pak, D. T. S., Sheng, M., et al. (2012). GKAP orchestrates activity-dependent postsynaptic protein remodeling and homeostatic scaling. *Nat. Neurosci.* 15, 1655–1666. doi: 10.1038/nn.3259

Sjöström, P. J., and Häusser, M. (2006). A cooperative switch determines the sign of synaptic plasticity in distal dendrites of neocortical pyramidal neurons. *Neuron* 51, 227–238. doi: 10.1016/j.neuron.2006.06.017

Sutton, M. A., Ito, H. T., Cressy, P., Kempf, C., Woo, J. C., and Schuman, E. M. (2006). Miniature neurotransmission stabilizes synaptic function via tonic suppression of local dendritic protein synthesis. *Cell* 125, 785–799. doi: 10.1016/j.cell.2006.03.040

Thiagarajan, T. C., Lindskog, M., and Tsien, R. W. (2005). Adaptation to synaptic inactivity in hippocampal neurons. *Neuron* 47, 725–737. doi: 10.1016/j.neuron.2005.06.037

Thiagarajan, T. C., Piedras-Renteria, E. S., and Tsien, R. W. (2002). α- and βCaMKII: inverse regulation by neuronal activity and opposing effects on synaptic strength. *Neuron* 36, 1103–1114. doi: 10.1016/S0896-6273(02)01049-8

Turrigiano, G. (2012). Homeostatic synaptic plasticity: local and global mechanisms for stabilizing neuronal function. *Cold Spring Harb. Perspect. Biol.* 4, 1–18. doi: 10.1101/cshperspect.a005736

Turrigiano, G. G. (2008). The self-tuning neuron: synaptic scaling of excitatory synapses. *Cell* 135, 422–435. doi: 10.1016/j.cell.2008.10.008

Turrigiano, G. G., and Nelson, S. B. (2000). Hebb and homeostasis in neuronal plasticity. *Curr. Opin. Neurobiol.* 10, 358–364. doi: 10.1016/S0959-4388(00)00091-X

Turrigiano, G. G., Leslie, K. R., Desai, N. S., Rutherford, L. C., and Nelson, S. B. (1998). Activity-dependent scaling of quantal amplitude in neocortical neurons. *Nature* 391, 892–896. doi: 10.1038/36103

Vest, R. S., Davies, K. D., O'Leary, H., Port, J. D., and Bayer, K. U. (2007). Dual mechanism of a natural CaMKII inhibitor. *Mol. Biol. Cell* 19, 308–317. doi: 10.1091/mbc.E07

Vigil, F. A., Mizuno, K., Lucchesi, W., Valls-Comamala, V., and Giese, K. P. (2017). Prevention of long-term memory loss after retrieval by an endogenous CaMKII inhibitor. *Sci. Rep.* 7:4040. doi: 10.1038/s41598-017-04355-8

Vlachos, A., Becker, D., Jedlicka, P., Winkels, R., Roeper, J., and Deller, T. (2012). Entorhinal denervation induces homeostatic synaptic scaling of excitatory postsynapses of dentate granule cells in mouse organotypic slice cultures. *PLoS One* 7:e32883. doi: 10.1371/journal.pone.0032883

Wang, C.-C., Held, R. G., Chang, S.-C., Yang, L., Delpire, E., Ghosh, A., et al. (2011). A critical role for GluN2B-Containing NMDA receptors in cortical development and function. *Neuron* 72, 789–805. doi: 10.1016/j.neuron.2011.09.023

Wierenga, C. J. (2005). Postsynaptic expression of homeostatic plasticity at neocortical synapses. *J. Neurosci.* 25, 2895–2905. doi: 10.1523/JNEUROSCI.5217-04.2005

Yang, X., Goldstein, A. M., Chase, G. A., Gastwirth, J. L., and Goldin, L. R. (2001). Use of weighted p-values in regional inference procedures. *Genet. Epidemiol.* 21, S484–S489. doi: 10.1002/gepi.2001.21.s1.s484